Inorganic Chemistry

Article

pubs.acs.org/IC

$K_2FeGe_3Se_8$: A New Antiferromagnetic Iron Selenide

Kai Feng,[†,‡,§] Wendong Wang,[▽] Ran He,[†,‡,§] Lei Kang,[†,‡,§] Wenlong Yin,[†,‡,§] Zheshuai Lin,[†,‡] Jiyong Yao,*[,†,‡] Youguo Shi,*[,⊥] and Yicheng Wu[†,‡]

[†]Center for Crystal Research and Development, Technical Institute of Physics and Chemistry, Chinese Academy of Sciences, Beijing 100190, People's Republic of China

[‡]Key Laboratory of Functional Crystals and Laser Technology, Technical Institute of Physics and Chemistry, Chinese Academy of Sciences, Beijing 100190, People's Republic of China

[§]Graduate University of the Chinese Academy of Sciences, Beijing 100049, People's Republic of China

[▽]School of Science, Beijing University of Post and Telecommunication, Beijing 100876, People's Republic of China

[⊥]Beijing National Laboratory for Condensed Matter Physics, Institute of Physics, Chinese Academy of Sciences, Beijing 100190, People's Republic of China

Supporting Information

ABSTRACT: A new iron selenide, $K_2FeGe_3Se_8$, has been obtained by spontaneous crystallization. It adopts a new structure type in the noncentrosymmetric monoclinic space group $P2_1$. In the structure, $FeSe_4$ and $GeSe_4$ tetrahedra are connected alternately via corner-sharing to form one-dimensional (1D) $^1_\infty[FeGeSe_6]^{6-}$ chains along the *a*-direction. These chains are further linked by sharing Ge_2Se_6 units to generate two-dimensional (2D) $^2_\infty[FeGe_3Se_8]^{2-}$ layers stacked parallel to the *ac*-plane and separated by K^+ cations. Deduced from temperature-dependent susceptibility measurement and specific heat measurement under different magnetic fields, $K_2FeGe_3Se_8$ exhibits an antiferromagnetic transition at ∼10 K. Furthermore, the magnetic property shows anisotropy between directions parallel and perpendicular to the plane of $^2_\infty[FeGe_3Se_8]^{2-}$ layer. The diffuse reflectance spectra measurement indicates that the band gap of $K_2FeGe_3Se_8$ is ∼1.95(2) eV, consistent with the calculated values of 1.80 and 1.53 eV in the spin-up and spin-down directions, respectively. Based on electronic structure calculation, the spin of the Fe^{2+} cation is 1.85$\hbar$, which is comparable to the experimental value.

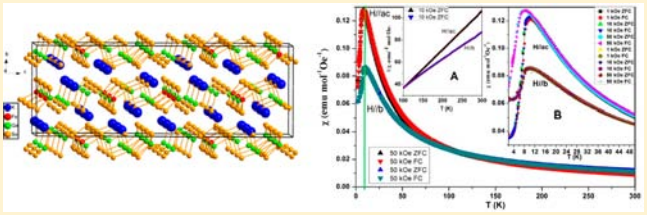

INTRODUCTION

Since the discovery of superconductivity in the quaternary Fe-based oxypnictide LaFePnO (Pn = pnictogen), there has been worldwide interest in Fe-based (oxy)pnictide and chalcogenides.[1−10] Until now, various Fe-based superconductors, such as the ZrCuSiAs-type oxypnictide LnFeAsO (Ln = rare-earth elements),[1,4,5] the $ThCr_2Si_2$-type AFe_2As_2 pnictide (A = alkaline-earth),[2,6] the Fe_2As-type AFeAs pnictide (A = Li, Na),[11,12] the anti-PbO-type chalcogenide FeSe,[3] and the intercalated chalcogenide AFe_2Se_2 (A = alkali-metal),[8−10,13] have been discovered and extensively studied, both experimentally and theoretically. The highest reported T_c = 55 K for iron-based superconductivity was achieved in oxygen-deficient SmFeAsO prepared via high-pressure synthesis.[5] These Fe-based superconductors exhibit fascinating interplay between the superconductivity and magnetism. A typical example is the AFe_2As_2 (A = alkaline-earth) pnictide system: the antiferromagnetic (AFM) order is suppressed and superconductivity is induced by either K doping in the Ba or Sr sites,[2,14] or by Co and Ni doping in the Fe sites,[15−17] or by applying pressure.[18] The high-critical-temperature (high-T_c) values, along with the proximity of a magnetically ordered state, suggest that the superconductivity in the Fe-based materials is unconventional and non-BCS-type.[19−21]

The fascinating properties of these Fe-based superconductors not only stimulate tremendous interest in optimizing experimental conditions to increase the T_c and in elucidating the electronic structure and superconducting mechanism, but also inspire intensive work in the exploratory synthesis of new Fe-based (oxy)pnictide and chalcogenides. Actually, the discovery of the superconductivity in the LaFePnO (Pn = pnictogen) clearly demonstrates the important role of exploratory synthesis in the development of modern materials science: without the initial synthesis and structural determination of the LaFePnO compounds in 1995,[22] no superconductivity could be found in Fe-based (oxy)pnictide and chalcogenides in ∼10 years later.[1] With great efforts, several new Fe-based (oxy)pnictide and chalcogenides has been synthesized, which show interesting structures and physical properties. For example, $CaFe_4As_3$ possesses an open three-dimensional framework built from $FeAs_4$ tetrahedra and exhibits metallic behavior with significant anisotropy and

Received: November 1, 2012
Published: January 28, 2013

   dx.doi.org/10.1021/ic302394e | *Inorg. Chem.* 2013, 52, 2022−2028

complex magnetic behavior,[23] $Fe_xPb_{4-x}Sb_4Se_{10}$ represents a new class of ferromagnetic semiconductors with quasi-one-dimensional (quasi-1D) ladders,[24] and the $RE_{12}Fe_{57.5}As_{41}$ (RE = La, Ce) compounds show ferromagnetic ordering at 125 and 95 K for the La and Ce compounds, respectively.[25]

To fully understand the structure−property relationship in solid-state chemistry and materials science, a materials database with a large number of related compounds is of great importance. In this context, we explored the A−Fe−M−Q system (A = alkali metal; M = Group IV element, Q = S, Se, Te) and discovered a new compound: $K_2FeGe_3Se_8$. In this work, we report the synthesis, structure, optical, specific heat, magnetic properties, and electronic structure calculations of $K_2FeGe_3Se_8$. This compound adopts a new structure type in the monoclinic space group $P2_1$ and exhibits an antiferromagnetic transition with a Neel temperature (T_N) of ∼10 K. The calculated spin of Fe^{2+} is 1.85$\hbar$, consistent with the experimental value. In addition, the calculated band gap is 1.80 and 1.53 eV in spin-up and spin-down directions, which is also consistent with the experiment.

EXPERIMENTAL SECTION

Crystal Growth. A mixture of K_2Se:FeSe:3$GeSe_2$, based on molar ratio, was loaded into a fused-silica tube under an argon atmosphere in a glovebox. The tube was sealed under 10^{-3} Pa atmosphere and then placed in a computer-controlled furnace. The sample was heated to 1173 K in 24 h and kept for 48 h, then cooled at a slow rate of 4 K/h to 673 K, and finally cooled to room temperature. The product consisted of thin dark-red plates of $K_2FeGe_3Se_8$, which were manually selected for structure characterization. Analysis of the crystal with an EDX-equipped Hitachi Model S-3500 scanning electron microscopy (SEM) system showed the presence of K, Fe, Ge, and Se in the approximate molar ratio of 2:1:3:8. The crystals are stable in air.

Structure Determination. Single-crystal X-ray diffraction data were collected with the use of graphite-monochromatized Mo Kα (λ = 0.71073 Å) at a temperature of 153 K on a Rigaku Model AFC10 diffractometer equipped with a Saturn CCD detector. Crystal decay was monitored by re-collecting 50 initial frames at the end of data collection. The collection of the intensity data was carried out with the program CrystalClear.[26] Cell refinement and data reduction were carried out with the use of the program CrystalClear,[26] and face-indexed absorption corrections were performed numerically with the use of the program XPREP.[27]

The structure was solved with the direct methods program SHELXS and refined with the least-squares program SHELXL of the SHELXTL.PC suite of programs.[27] Because of the strong layer tendency in the structure, the selected thin plate-shaped crystal was heavily twinned with fractional contributions of domains being 0.34, 0.33, 0.27, and 0.05. The high linear absorption coefficient (25.46 mm^{-1}) and the crystal twinning make the absorption correction difficult, which may explain why the final R/wR_2 values were relatively high. Additional experimental details are given in Table 1, and selected metric data are given in Table 2. Further information may be found in the Supporting Information.

Diffuse Reflectance Spectroscopy. A Cary Model 5000 ultraviolet−visible light−near-infrared (UV-vis-NIR) spectrophotometer with a diffuse reflectance accessory was used to measure the spectrum of $K_2FeGe_3Se_8$ over the range from 300 nm (4.13 eV) to 1500 nm (0.83 eV).

Magnetic Susceptibility Measurements. The temperature dependence of the magnetic susceptibility was measured on single crystals of $K_2FeGe_3Se_8$ (6.3 mg for $H//ac$ and 10.8 mg for $H//b$) in magnetic fields of 1, 10, and 50 kOe with the use of a superconducting quantum interference device (SQUID) magnetometer (Model MPMS7T, Quantum Design). The zero-field-cooled (ZFC) and field-cooled (FC) magnetic susceptibilities were obtained on crystals in the temperature range of 2−300 K. The field dependence of magnetization was measured at 2, 5, 10, 30, and 300 K by changing the applied magnetic field between −50 kOe and 50 kOe.

Table 1. Crystal Data and Structure Refinements for $K_2FeGe_3Se_8$

parameter	value/comment
chemical formula	$K_2FeGe_3Se_8$
formula weight, fw	983.500
uni-cell dimensions	
a	7.4088(15) Å
b	12.268(3) Å
c	34.974(7) Å
β	96.04(3)°
V	3161.3(11) Å^3
space group	$P2_1$
Z	8
T	153(2) K
λ	0.71073 Å
ρ_c	4.133 g/cm^3
μ	25.460 cm^{-1}
$R(F)^a$	0.0799
$R_W(F_o^2)^b$	0.2030

$^aR(F) = \sum||F_o| - |F_c||/\sum|F_o|$ for $F_o^2 > 2\sigma(F_o^2)$. $^bR_w(F_o^2) = \{\sum[w(F_o^2 - F_c^2)^2]/\sum wF_o^4\}^{1/2}$ for all data. $w^{-1} = \sigma^2(F_o^2) + (zP)^2$, where $P = (\mathrm{Max}(F_o^2, 0) + 2F_c^2)/3$.

Table 2. Selected Interatomic Distances for $K_2FeGe_3Se_8$

atom pair	bond distance (Å)	atom pair	bond distance (Å)
Fe1−Se7	2.425(5)	Ge4−Se5	2.308(5)
Fe1−Se6	2.454(6)	Ge4−Se6	2.358(5)
Fe1−Se2	2.474(5)	Ge4−Se3	2.377(5)
Fe1−Se5	2.485(6)	Ge4−Se1	2.404(4)
Fe2−Se4	2.379(6)	Ge5−Se26	2.295(5)
Fe2−Se9	2.417(6)	Ge5−Se15	2.375(4)
Fe2−Se21	2.493(5)	Ge5−Se16	2.385(6)
Fe2−Se22	2.501(6)	Ge5−Se13	2.388(4)
Fe3−Se30	2.416(6)	Ge6−Se27	2.322(5)
Fe3−Se23	2.439(5)	Ge6−Se12	2.367(4)
Fe3−Se32	2.467(6)	Ge6−Se28	2.380(6)
Fe3−Se27	2.492(5)	Ge6−Se14	2.388(4)
Fe4−Se19	2.455(6)	Ge7−Se19	2.292(5)
Fe4−Se31	2.464(6)	Ge7−Se25	2.358(5)
Fe4−Se29	2.470(6)	Ge7−Se20	2.393(6)
Fe4−Se26	2.474(5)	Ge7−Se11	2.393(4)
Ge1−Se22	2.300(5)	Ge8−Se32	2.307(5)
Ge1−Se24	2.353(5)	Ge8−Se30	2.325(5)
Ge1−Se8	2.392(4)	Ge8−Se12	2.389(5)
Ge1−Se10	2.403(5)	Ge8−Se18	2.426(4)
Ge2−Se21	2.291(5)	Ge9−Se31	2.297(5)
Ge2−Se17	2.372(5)	Ge9−Se29	2.335(5)
Ge2−Se15	2.382(6)	Ge9−Se13	2.392(5)
Ge2−Se16	2.403(4)	Ge9−Se25	2.428(5)
Ge3−Se23	2.274(5)	Ge10−Se7	2.312(5)
Ge3−Se18	2.351(4)	Ge10−Se1	2.342(5)
Ge3−Se8	2.389(5)	Ge10−Se20	2.383(4)
Ge3−Se10	2.407(4)	Ge10−Se11	2.403(6)
Ge12−Se2	2.307(5)	Ge11−Se9	2.280(5)
Ge12−Se14	2.377(6)	Ge11−Se4	2.307(5)
Ge12−Se3	2.379(5)	Ge11−Se17	2.427(5)
Ge12−Se28	2.388(4)	Ge11−Se24	2.464(5)

dx.doi.org/10.1021/ic302394e | Inorg. Chem. 2013, 52, 2022−2028

Specific Heat Measurement. Specific heat capacity (C_p) versus temperature (T) of $K_2FeGe_3Se_8$ was recorded at 2−300 K (ZFC) and 0−15 K for 20, 40, 70, and 90 kOe magnetic fields by a pulse relaxation method, using a Quantum Design Model PPMS calorimeter.

Electronic Structure Calculations. The first-principles calculation for $K_2FeGe_3Se_8$ was performed by the plane-wave pseudopotential method based on the density functional theory (DFT).[28,29] The CASTEP package[30] was employed to determine the electronic structures, including total density of states (DOS) and partial DOS (PDOS). The ion−electron interactions were modeled by the optimized ultrasoft pseudo-potentials[31] for elements in the compound. The adopted density functional is an additional on-site orbital-dependent correlation Hubbard U (LDA + U), and the DOS presented here are those adopting U values of 2.5 eV only for Fe^{2+}. In addition, the magnetic moment of the crystal is determined by the spin-polarized calculations.[32] The kinetic energy cutoffs of 500 eV and Monkhorst−Pack k-point meshes with the spanning of <0.07/Å^3 in the Brillouin zone were chosen.[33] Other calculating parameters and convergent criterions were set by the default values of CASTEP code. Our tests reveal that the above computational parameters are sufficiently accurate for present purposes.

RESULTS AND DISCUSSION

Synthesis. The new iron selenide, $K_2FeGe_3Se_8$, has been synthesized by traditional high-temperature solid-state reaction for the first time. The yield was ∼50%, based on Fe. Great efforts have been made to synthesize analogues containing other alkali-metal, Group IV element, or chalcogen available to us, such as Na, Si, Sn, S, and Te, but they did not work. The differences in atomic coordination environments and ionic radii have a significant effect on the stability of crystal structure, which may be the reason why the attempts to synthesize similar compounds from the Na, Si, Sn, S, and Te were not successful.

Crystal Structure. As shown in Figure 1B, $K_2FeGe_3Se_8$ crystallizes in a new structure type in noncentrosymmetric space group $P2_1$ of the monoclinic system. There are 8 crystallographically independent K atoms, 4 independent Fe atoms, 12 independent Ge atoms, and 32 independent Se atoms in the asymmetric unit, all at general sites 2a (Figure 1A). Without Se−Se and metal−metal bonds in the structure, the oxidation states of 1+, 2+, 4+, and 2− can be assigned to K, Fe, Ge, and Se, respectively.

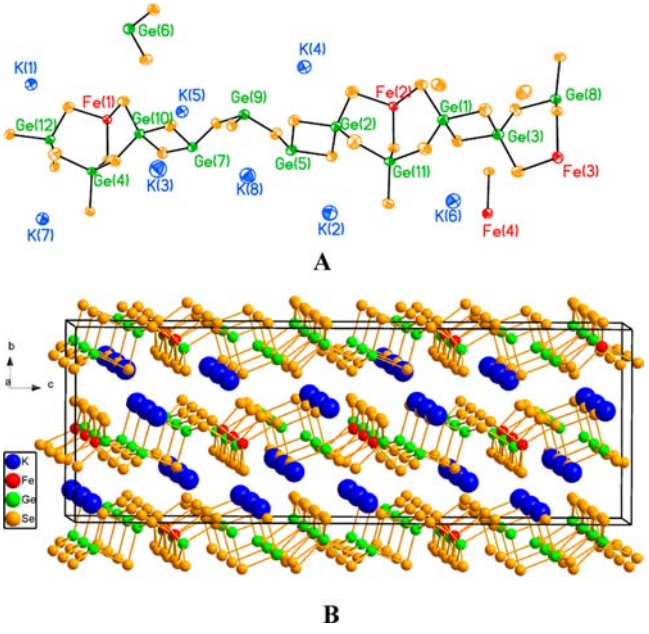

Figure 1. (A) Asymmetric unit of $K_2FeGe_3Se_8$ (the displacement ellipsoids are shown at the 90% probability level) and (B) crystal structure of $K_2FeGe_3Se_8$ viewed down the a-direction.

The basic structure units in $K_2FeGe_3Se_8$ are $FeSe_4$ and $GeSe_4$ tetrahedra, which are connected alternately by sharing corner Se atoms to form a one-dimensional (1D) $^1_\infty[FeGeSe_6]^{6-}$ anionic chain along the a-axis. (Figure 2) The chains then

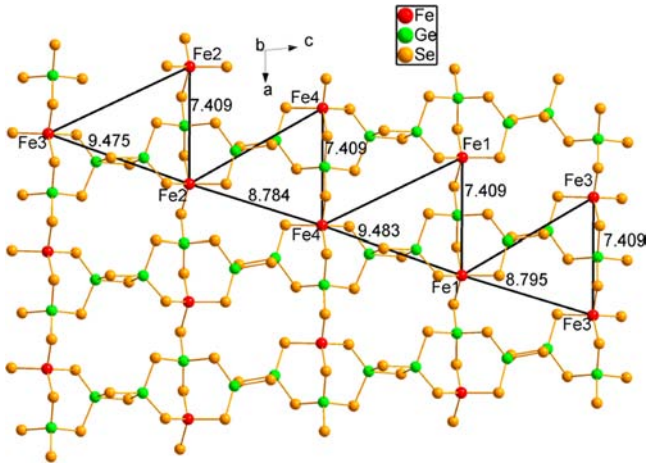

Figure 2. Structure of an infinite layer $^2_\infty[FeGe_3Se_8]^{2-}$ arranged in the ac-plane with the intrachain and interchain Fe···Fe distances shown (distances are given in units of Å).

are further linked with each other via sharing $[Ge_2Se_6]^{4-}$ anion groups, built from two $GeSe_4$ tetrahedra via sharing edges, along the c-direction to generate $^2_\infty[FeGe_3Se_8]^{2-}$ layers. The layers are stacked along the b-direction and separated by K^+ cations.

In $K_xFe_2Se_2$[8] and FeSe,[34] $FeSe_4$ tetrahedra are linked with each other via edge-sharing to form 2D layers. However, in $K_2FeGe_3Se_8$, $FeSe_4$ tetrahedra are not joined with each other directly, but are connected by $GeSe_4$ tetrahedra along the a-direction. Moreover, it is interesting to note that, although there are four types of crystallographically unique $^1_\infty[FeGeSe_6]^{6-}$ chains in the structure, the shortest intrachain Fe···Fe distances within each chain are all the same and equal to the length of the a-axis, 7.409(2) Å (Figure 2). The $^1_\infty[FeGeSe_6]^{6-}$ chains are further connected to each other by the $[Ge_2Se_6]^{4-}$ groups, resulting in the $^2_\infty[FeGe_3Se_8]^{2-}$ layers. The shortest interchain Fe···Fe distances among the unique Fe atoms within the $^2_\infty[FeGe_3Se_8]^{2-}$ layer are 8.795 (2) Å between the Fe3 cation and the Fe1 cation, 9.483(2) Å between the Fe1 cation and the Fe4 cation, 8.784(2) Å between the Fe4 cation and the Fe2 cation, and 9.475(3) Å between the Fe2 cation and the Fe3 cation. Furthermore, these Fe cations, whose positions could achieve the shortest interchain Fe···Fe distance, are also aligned approximately along a straight line, with the angle Fe3−Fe1−Fe4 being 176.89(2)°, the angle Fe1−Fe4−Fe2 being 177.49(2)°, and the angle Fe4−Fe2−Fe3 being 177.53(2)° (see Figure 2). Thus, the arrangement of $FeSe_4$ tetrahedra within the $^2_\infty[FeGe_3Se_8]^{2-}$ layer is quite regular in this compound. Such an arrangement is observed for the first time in iron selenide. As for two adjacent $^2_\infty[FeGe_3Se_8]^{2-}$ layers, the shortest interlayer Fe···Fe distances among the unique Fe atoms are 6.917 (2) Å between two Fe2 atoms, 6.921(1) Å between two Fe1 atoms, 7.160(2) Å between the Fe4 atom and

dx.doi.org/10.1021/ic302394e | Inorg. Chem. 2013, 52, 2022−2028

the Fe3 atom, and 8.452(2) Å between the Fe4 atom and the Fe2 atom.

Selected bond distances for $K_2FeGe_3Se_8$ are listed in Table 2. The distances of Fe−Se bonds range from 2.379(6) Å to 2.501(6) Å, which are similar to those for tetrahedrally coordinated Fe in $K_3Fe_2Se_4$ (2.402(4)−2.465(3) Å)[35] and $K_xFe_2Se_2$ ($0 \le x \le 1$) (2.4406(4) Å),[8] and are slightly longer than those in FeSe (2.300(2) Å).[34] The Se−Fe−Se angles for $K_2FeGe_3Se_8$ range from 94.3(2)° to 116.88(19)°; in comparison, Se−Fe−Se angles within the $FeSe_4$ tetrahedra range from 106.600(4)° to 110.926(4)° for $K_xFe_2Se_2$,[8] from 103.218(4)° to 112.903(5)° for FeSe,[34] and from 101.52(9)° to 115.24(11)° for $K_3Fe_2Se_4$.[35] Given the ranges of the bond lengths and angles, the $FeSe_4$ tetrahedra of $K_2FeGe_3Se_8$ are more distorted than those in $K_3Fe_2Se_4$, $K_xFe_2Se_2$, and FeSe. The lengths of the Ge−Se bonds in $K_2FeGe_3Se_8$ range from 2.274(5) Å to 2.464(5) Å, which is comparable to those for tetrahedrally coordinated Ge in K_2GeSe_4 (2.275(5)−2.432(5) Å),[36] $KCeGeSe_4$ (2.316(2)−2.355(1) Å),[37] and $Li_2In_2GeSe_6$ (2.314(1)−2.331(1) Å).[38] The $GeSe_4$ tetrahedra is also obviously distorted as the Se−Ge−Se angles lie in the wide range of 96.52(15)°−118.70(19)°. As for the K−Se bond lengths, they are normal, ranging from 3.232(7) Å to 3.912(8) Å, which is comparable to those in $KGaSe_2$ (3.322(2)−3.917(2) Å).[39]

The calculated bond valence sums (BVS)[40] of all cations for $K_2FeGe_3Se_8$ are listed in Table 3. All K cations are

Table 3. Band Valence in $K_2FeGe_3Se_8$

site	valence	site	valence
K1	0.92	Ge1	3.79
K2	0.79	Ge2	3.75
K3	0.72	Ge3	3.82
K4	0.85	Ge4	3.75
K5	0.87	Ge5	4.03
K6	0.87	Ge6	3.74
K7	0.76	Ge7	3.81
K8	0.77	Ge8	3.87
Fe1	2.48	Ge9	3.84
Fe2	2.45	Ge10	3.80
Fe3	2.27	Ge11	3.78
Fe4	2.40	Ge12	4.00

underbonded, with BVS values in the range of 0.72−0.92. The BVS values of Fe are 2.27−2.48, which indicates that all Fe are overbonded. Similar values are also found in $BaFe_2Se_3$[41] (the BVS value of Fe is 2.755), $Fe_2In_2Se_5$[42] (the BVS value of Fe with a tetrahedral coordination environment is 2.512), and $BaFe_2OSe_2$[43] (the BVS value of Fe is 2.23). Most of the Ge atoms are slightly underbonded (BVS = 3.74−3.87), while the Ge5 and Ge12 atoms have BVS values close to the expected values (4.00 and 4.03, respectively).

Magnetic Susceptibility Measurements. Magnetization data, collected as a function of temperature for $K_2FeGe_3Se_8$ ($H//ac$ and $H//b$), are shown in Figure 3, which indicates an antiferromagnetic transition at T_N = 10 K. In addition, the inset shown as inset A in Figure 3 depicts the inverse magnetic susceptibility ($1/\chi$), as a function of temperature (T), for 10 kOe. This antiferromagnetic transition should be attributable to the antiferromagnetic order of the Fe^{2+} cation, which is the only magnetic ion in the compound. The susceptibility data were used to fit the Curie−Weiss equation,

$$\chi = \frac{C}{T - \theta}$$

where C is the Curie constant and θ is the Weiss constant; the effective magnetic moments (μ_{eff}) were evaluated from the equation[44]

$$\mu_{eff} = \sqrt{8C}\,\mu_B$$

The temperature range of 100−300 K provided the best linear fit to the data and were used to extract these values. Curie−Weiss fitting of our data yields values of C and θ are 2.94 emu K/mol and −6.38 K, respectively, for $H//ac$ and 3.84 emu K/mol and −43.04 K, respectively, for $H//b$. Moreover, the calculated μ_{eff} values are $4.85\mu_B$ and $5.54\mu_B$ for $H//ac$ and $H//b$, respectively. The μ_{eff} for $H//ac$ is quite close to the expected value for Fe^{2+} (S = 2) ($\mu_{eff} = 4.92\mu_B$) in high-spin state.[45] However, on the other hand, the μ_{eff} value for $H//b$ is obviously higher than the normal value and the corresponding θ value is lower, which indicates that the exchange interaction along the b-direction is stronger. The magnetic anisotropy is quite understandable when we take its crystal structure, which is far away from cubic symmetry, into consideration. As discussed in the structure description, the shortest interlayer ($//b$) Fe···Fe distance is much shorter than the shortest intralayer ($//ac$) Fe···Fe distance. As a result, magnetic interaction between the ac-plane becomes stronger, causing higher μ_{eff} along the b-axis than that along the ac-plane. The magnetic anisotropy shows some complexity but is not unpredictable below T_N and under high magnetic fields. As shown in inset B in Figure 3, the susceptibility along the b-axis has no evident dependence on magnetic field up to 50 kOe, but the susceptibility along the ac-plane shows great difference between lower and higher fields. In principle, all antiferromagnetic order can be killed by sufficient high fields and show ferromagnetism. Our results shown in inset B in Figure 3 clearly manifest the AFM−FM transition along the b-axis will be at much higher field than that along the ac-plane, proving again that the exchange interaction along the b-direction is quite strong.

The AFM transition temperature is ∼10 K, which is further confirmed by the curve of magnetization (M) versus applied field (H), operated in 2, 5, 10, 30, and 300 K for $H//ac$ and $H//b$ (see Figure 4). It can be seen that the curve of 10 K has the largest slope, namely, χ. The magnetization is 1.12 and 0.78 μ_B/Fe^{2+} for $H//ac$ and $H//b$ at 10 K, 23% and 16% of the expected magnetic moment of the high spin state Fe^{2+}, which is most likely due to a Dzyaloshinsky−Moriya interaction generated by the broken inversion symmetry.[46] In addition, no obviously magnetic hysteresis loop is observed for $H//b$ (see Figure 4). However, for $H//ac$, a slope change in the H−M curve at 2 and 5 K can be seen clearly at 40 kOe and 30 kOe, respectively. Such anisotropy can also be explained with respect to the crystal structure. As discussed earlier, with regard to the anisotropy of susceptibility, the exchange interaction along the b-axis is stronger than that along the ac-plane, so the AFM order along the ac-plane is easier to be destroyed with moderate fields above 30 kOe and begins to show ferromagnetism under high fields, while the AFM state along the b-axis can persist at higher magnetic fields. The AFM anisotropy phenomenon in $K_2FeGe_3Se_8$ single crystals is so interesting that it is worthwhile to be further investigated using other methods, such as neutron diffraction.

dx.doi.org/10.1021/ic302394e | Inorg. Chem. 2013, 52, 2022−2028

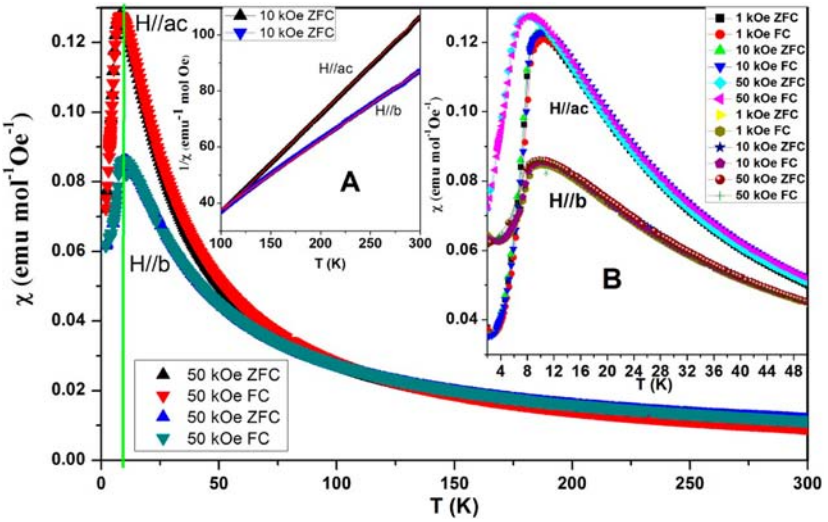

Figure 3. Magnetic susceptibility (χ) versus temperature (T) of $K_2FeGe_3Se_8$ under applied fields of 1, 10, and 50 kOe. Inset A shows the plot of $1/\chi$ versus T from T = 100 K to T = 300 K ($H//b$ and $H//ac$). Inset B shows the $\chi(T)$ curves at low temperature.

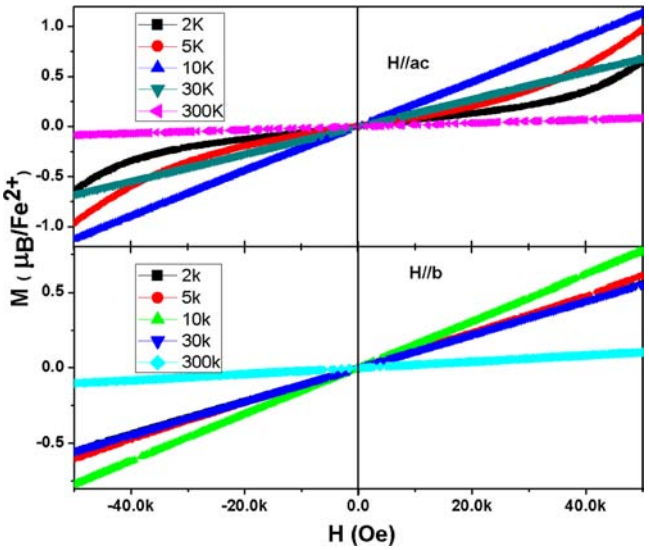

Figure 4. $M-H$ curves of $K_2FeGe_3Se_8$ at temperatures of 2, 5, 10, 30, and 300 K ($H//b$ and $H//ac$).

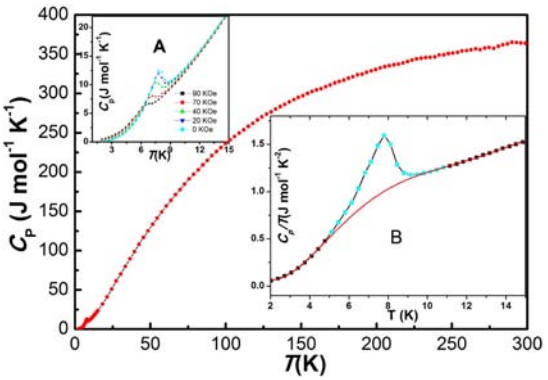

Figure 5. Curves of heat capacity (C_p) versus temperature (T) of $K_2FeGe_3Se_8$. Inset A shows the plot of specific heat versus temperature with different fields. Inset B shows an expanded view of the data in the vicinity of the peak.

Specific Heat Measurement. Figure 5 plots C_P vs T for the $K_2FeGe_3Se_8$ sample in zero magnetic fields from 2 K to 300 K. The specific heat measurement shows a λ-type anomaly at ~9.3 K, which is ascribed to the antiferromagnetic transition and indicates that the magnetic transition is of a bulk nature.

Inset A in Figure 5 displays the low-temperature curve of the specific heat capacity $C_P(T)$ under different magnetic fields (0, 20, 40, 70, and 90 kOe). There is a clear jump in specific heat close to 10 K, which is consistent with the sharp magnetic susceptibility peak; this clearly suggests an AFM transition. The C_P peak shifted to lower temperature and became screened little by little with increasing field, which is expected from an AFM−FM transition, as discussed in the magnetic results for Figures 3 and 4. Evidently, at low fields, the temperature dependence of C_P shows an AFM transition, while at higher fields, especially above 90 kOe (Figure 5), $K_2FeGe_3Se_8$ almost becomes ferromagnetic within the entire experimental temperature range and does not show clear AFM transition anymore.

As shown in inset B in Figure 5, the peak part was generally separated from the body of the C_p data through a polynomial function. The entropy change is calculated to be 1.18 J mol^{-1} K^{-1}, which is ~8% of the expected value (R ln(2S + 1), where R is the ideal gas constant and, here, S = 2); most of the entropy is removed via short-range ordering above T_N.

Experimental Band Gaps. Based on the UV-vis-NIR diffuse reflectance spectra of $K_2FeGe_3Se_8$ (Figure 6), the band gap can be deduced via the straightforward extrapolation method.[47] Obviously, the absorption edge of $K_2FeGe_3Se_8$ is ~635 nm and is consistent with the dark-red color of material.

Electronic Structure Calculations. To gain better insight into the electronic structure and bond properties of $K_2FeGe_3Se_8$, the density of states (DOS) and partial density of states (PDOS) are calculated by the spin-polarized LDA + U method and plotted in Figures 7A and 7B, respectively, which clearly displays the s, p, and d orbitals of constituent elements, especially of Fe atoms and their respective contributions to the total band structure. The analyses show that, in different polarized directions (corresponding to spin up and spin down, as shown in Figures 7A and 7B), the s and p orbitals of potassium (K), germanium (Ge), and selenium (Se) atoms, which concentrate at about −12 eV, −8 eV, and the upper

dx.doi.org/10.1021/ic302394e | Inorg. Chem. 2013, 52, 2022−2028

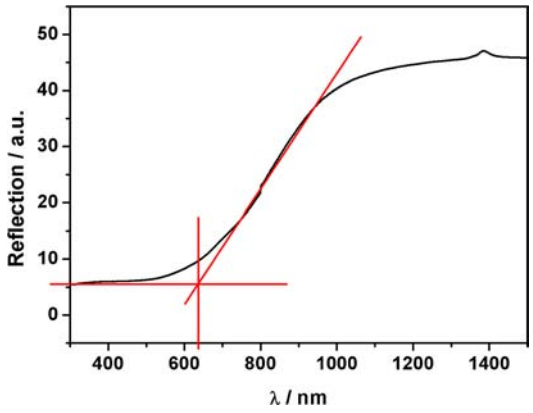

Figure 6. Diffuse reflectance spectrum of $K_2FeGe_3Se_8$.

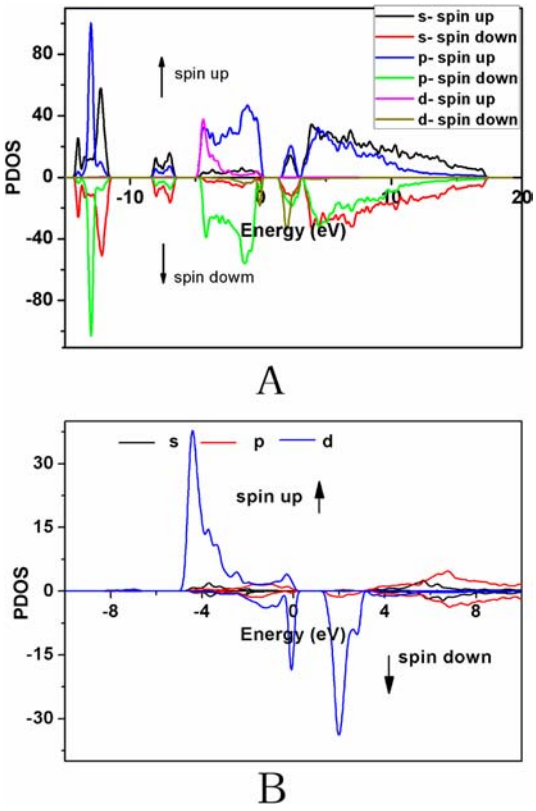

Figure 7. (A) PDOS projected on all atoms in $K_2FeGe_3Se_8$ and (B) orbital-resolved spin-polarized PDOS on Fe 3d orbitals of $K_2FeGe_3Se_8$.

region of valence band (VB), have almost similar contribution to the band structure, while the d orbitals from Fe atoms behave very differently: they are located at about −4 eV and +2 eV in the spin-up direction and spin-down direction, respectively. However, the calculated energy band gaps are similar. In the spin-up direction, the calculated band gap is 1.80 eV, and in the spin-down direction, it is 1.53 eV, which are in good agreement with experimental measurement. In addition, the maximum of VB is mostly occupied by the p orbitals of Se atoms and the s orbitals of Ge atoms, which contribute the most to the optical effect. The hybrid of s−p orbitals of Ge and Fe and the overlap of p−p orbitals in Ge−Se and Fe−Se, respectively, exhibit that the chemical bonds of Se−Ge and Se−Fe are produced and display the style of tetrahedron (see Figure 7A).

Since the Fe−Se bond lengths (2.379(6)−2.501(6) Å) are obviously larger than the sum of ion radius of Fe^{2+} and Se^{2-}, there is no significant splitting of the d orbitals, which indicates a weak tetrahedral field in $K_2FeGe_3Se_8$. As a result, two of the six d electrons occupy one d orbital and other four remaining d-electrons occupy the other four d orbitals, with the total spin being $2\hbar$. The calculated result shows that the spin of Fe^{2+} is $\sim 1.85-1.86\hbar$, which agrees with the experimental magnetic measurements very well.

CONCLUSION

A new antiferromagnetic compound, $K_2FeGe_3Se_8$, has been synthesized. It crystallizes in the noncentrosymmetric space group $P2_1$ of the monoclinic system. The structure is built from $GeSe_4$ and $FeSe_4$ tetrahedra, which are connected to each other alternatively to generate a one-dimensional (1D) $^1_\infty[FeGeSe_6]^{6-}$ chain, and then the chains are linked further by sharing Ge_2Se_6 anionic group to form two-dimensional (2D) $^2_\infty[FeGe_3Se_8]^{2-}$ layers with interspace occupied by K^+ cations. The compound exhibits an antiferromagnetic (AFM) transition at ∼10 K, which is confirmed by the temperature dependence of the magnetic susceptibilities measurement and field dependence of magnetization measurement. The $H-M$ curves of $K_2FeGe_3Se_8$ show anisotropy, and the band gap is deduced to 1.95 eV by UV-vis-NIR diffuse reflectance. The theoretical calculated results reveal that, in $K_2FeGe_3Se_8$, the Fe^{2+} cation shows high spin with four lone electrons. In the spin-up and spin-down directions, the theory band gap is 1.80 and 1.53 eV, respectively. This compound, with its interesting structures and properties, may be a valuable addition to the family of iron-based chalcogenides.

ASSOCIATED CONTENT

Supporting Information

Crystallographic file in CIF format for $K_2FeGe_3Se_8$. This material is available free of charge via the Internet at http://pubs.acs.org.

AUTHOR INFORMATION

Corresponding Author

*E-mails: jyao@mail.ipc.ac.cn (J.Y.), ygshi@aphy.iphy.ac.cn (Y.S.).

Notes

The authors declare no competing financial interest.

ACKNOWLEDGMENTS

This research was supported by the National Basic Research Project of China (No. 2010CB630701), National Natural Science Foundation of China (No. 91122034 and 51102249), and the Ministry of Science and Technology of China (973 Project No. 2011CBA00110). We thank Dr. Jun Lu, who is a senior engineer from the State Key Laboratory of Magnetism in IOP−CAS, for useful discussions concerning magnetic-related results.

REFERENCES

(1) Kamihara, Y.; Hiramatsu, H.; Hirano, M.; Kawamura, R.; Yanagi, H.; Kamiya, T.; Hosono, H. *J. Am. Chem. Soc.* **2006**, *128*, 10012−10013.

(2) Chen, G.-F.; Li, Z.; Li, G.; Hu, W.-Z.; Dong, J.; Zhou, J.; Zhang, X.-D.; Zheng, P.; Wang, N.-L.; Luo, J.-L. *Chin. Phys. Lett.* **2008**, *25*, 3403−3405.

(3) Hsu, F.-C.; Luo, J.-Y.; Yeh, K.-W.; Chen, T.-K.; Huang, T.-W.; Wu, P. M.; Lee, Y.-C.; Huang, Y.-L.; Chu, Y.-Y.; Yan, D.-C.; Wu, M.-K. *Proc. Natl. Acad. Sci. U.S.A.* **2008**, *105*, 14262−14264.
(4) Kamihara, Y.; Watanabe, T.; Hirano, M.; Hosono, H. *J. Am. Chem. Soc.* **2008**, *130*, 3296−3297.
(5) Ren, Z.-A.; Che, G.-C.; Dong, X.-L.; Yang, J.; Lu, W.; Yi, W.; Shen, X.-L.; Li, Z.-C.; Sun, L.-L.; Zhou, F.; Zhao, Z.-X. *Europhys. Lett.* **2008**, 83.
(6) Ronning, F.; Klimczuk, T.; Bauer, E. D.; Volz, H.; Thompson, J. D. *J. Phys.: Condens. Matter* **2008**, 20.
(7) Takahashi, H.; Igawa, K.; Arii, K.; Kamihara, Y.; Hirano, M.; Hosono, H. *Nature* **2008**, *453*, 376−378.
(8) Guo, J.; Jin, S.; Wang, G.; Wang, S.; Zhu, K.; Zhou, T.; He, M.; Chen, X. *Phys. Rev. B* **2010**, 82.
(9) Fang, M.-H.; Wang, H.-D.; Dong, C.-H.; Li, Z.-J.; Feng, C.-M.; Chen, J.; Yuan, H. Q. *Europhys. Lett.* **2011**, 94.
(10) Mizuguchi, Y.; Takeya, H.; Kawasaki, Y.; Ozaki, T.; Tsuda, S.; Yamaguchi, T.; Takano, Y. *Appl. Phys. Lett.* **2011**, 98.
(11) Wang, X. C.; Liu, Q. Q.; Lv, Y. X.; Gao, W. B.; Yang, L. X.; Yu, R. C.; Li, F. Y.; Jin, C. Q. *Solid State Commun.* **2008**, *148*, 538−540.
(12) Chu, C. W.; Chen, F.; Gooch, M.; Guloy, A. M.; Lorenz, B.; Lv, B.; Sasmal, K.; Tang, Z. J.; Tapp, J. H.; Xue, Y. Y. *Physica C* **2009**, *469*, 326−331.
(13) Ksenofontov, V.; Medvedev, S. A.; Schoop, L. M.; Wortmann, G.; Palasyuk, T.; Tsurkan, V.; Deisenhofer, J.; Loidl, A.; Felser, C. *Phys. Rev. B* **2012**, 85.
(14) Rotter, M.; Tegel, M.; Johrendt, D. *Phys. Rev. Lett.* **2008**, 101.
(15) Leithe-Jasper, A.; Schnelle, W.; Geibel, C.; Rosner, H. *Phys. Rev. Lett.* **2008**, 101.
(16) Sefat, A. S.; Jin, R.; McGuire, M. A.; Sales, B. C.; Singh, D. J.; Mandrus, D. *Phys. Rev. Lett.* **2008**, *101*, 117004.
(17) Kasinathan, D.; Ormeci, A.; Koch, K.; Burkhardt, U.; Schnelle, W.; Leithe-Jasper, A.; Rosner, H. *New J. Phys.* **2009**, 11.
(18) Kumar, M.; Nicklas, M.; Jesche, A.; Caroca-Canales, N.; Schmitt, M.; Hanfland, M.; Kasinathan, D.; Schwarz, U.; Rosner, H.; Geibel, C. *Phys. Rev. B* **2008**, *78*, 184516.
(19) Luetkens, H.; Klauss, H. H.; Khasanov, R.; Amato, A.; Klingeler, R.; Hellmann, I.; Leps, N.; Kondrat, A.; Hess, C.; Koehler, A.; Behr, G.; Werner, J.; Buechner, B. *Phys. Rev. Lett.* **2008**, 101.
(20) Nakai, Y.; Ishida, K.; Kamihara, Y.; Hirano, M.; Hosono, H. *J. Phys. Soc. Jpn.* **2008**, 77.
(21) Shan, L.; Wang, Y. L.; Zhu, X. Y.; Mu, G.; Fang, L.; Ren, C.; Wen, H. H. *Europhys. Lett.* **2008**, 83.
(22) Zimmer, B. I.; Jeitschko, W.; Albering, J. H.; Glaum, R.; Reehuis, M. *J. Alloys Compd.* **1995**, *229*, 238−242.
(23) Todorov, I.; Chung, D. Y.; Malliakas, C. D.; Li, Q. a.; Bakas, T.; Douvalis, A.; Trimarchi, G.; Gray, K.; Mitchell, J. F.; Freeman, A. J.; Kanatzidis, M. G. *J. Am. Chem. Soc.* **2009**, *131*, 5405.
(24) Poudeu, P. F. P.; Takas, N.; Anglin, C.; Eastwood, J.; Rivera, A. *J. Am. Chem. Soc.* **2010**, *132*, 5751−5760.
(25) Stoyko, S. S.; Blanchard, P. E. R.; Mar, A. *Inorg. Chem.* **2010**, *49*, 2325−2333.
(26) R. Corporation. *CrystalClear*. Tokyo, 2008.
(27) Sheldrick, G. M. *Acta Crystallogr., Sect. A: Found. Crystallogr.* **2008**, *64*, 112−122.
(28) Kohn, W.; Sham, L. J. *Phys. Rev.* **1965**, *140*, 1133.
(29) Payne, M. C.; Teter, M. P.; Allan, D. C.; Arias, T. A.; Joannopoulos, J. D. *Rev. Mod. Phys.* **1992**, *64*, 1045−1097.
(30) Clark, S. J.; Segall, M. D.; Pickard, C. J.; Hasnip, P. J.; Probert, M. J.; Refson, K.; Payne, M. C. *Z. Kristallogr.* **2005**, *220*, 567−570.
(31) Vanderbilt, D. *Phys. Rev. B* **1990**, *41*, 7892−7895.
(32) Perdew, J. P.; Zunger, A. *Phys. Rev. B* **1981**, *23*, 5048−5079.
(33) Monkhorst, H. J.; Pack, J. D. *Phys. Rev. B* **1976**, *13*, 5188−5192.
(34) Margadonna, S.; Takabayashi, Y.; Ohishi, Y.; Mizuguchi, Y.; Takano, Y.; Kagayama, T.; Nakagawa, T.; Takata, M.; Prassides, K. *Phys. Rev. B* **2009**, 80.
(35) Bronger, W.; Genin, H. S.; Muller, P. *Z. Anorg. Allg. Chem.* **1999**, *625*, 274−278.
(36) Sheldrick, W. S.; Schaaf, B. *Z. Naturforsch., B: Chem. Sci.* **1995**, *50*, 1469−1475.
(37) Choudhury, A.; Polyakova, L. A.; Hartenbach, I.; Schleid, T.; Dorhout, P. K. *Z. Anorg. Allg. Chem.* **2006**, *632*, 2395−2401.
(38) Yin, W.; Feng, K.; Hao, W.; Yao, J.; Wu, Y. *Inorg. Chem.* **2012**, *51*, 5839−5843.
(39) Feng, K.; Mei, D.; Bai, L.; Lin, Z.; Yao, J.; Wu, Y. *Solid State Sci.* **2012**, *14*, 1152−1156.
(40) Brown, I. D.; Altermatt, D. *Acta Crystallogr., Sect. B: Struct. Sci.* **1985**, *41*, 244−247.
(41) Krzton-Maziopa, A.; Pomjakushina, E.; Pomjakushin, V.; Sheptyakov, D.; Chernyshov, D.; Svitlyk, V.; Conder, K. *J. Phys.: Condens. Matter* **2011**, 23.
(42) Cedeno, C.; de Delgado, G. D.; Delgado, J. M.; de Chalbaud, L. M.; Sagredo, V. *J. Phys. Chem. Solids* **2005**, *66*, 2049−2051.
(43) Lei, H.; Ryu, H.; Ivanovski, V.; Warren, J. B.; Frenkel, A. I.; Cekic, B.; Yin, W.-G.; Petrovic, C. *Phys. Rev. B* **2012**, 86.
(44) O'Connor, C. J. *Magnetochemistry—Advances in Theory and Experimentation*; Lippard, S. J., Ed.; Progress in Inorganic Chemistry, Vol. *29*; John Wiley & Sons, Inc.: Hoboken, NJ, 2007; pp 203−283.
(45) Schmid, H.; Rieder, H.; Ascher, E. *Solid State Commun.* **1965**, *3*, 327−330.
(46) Moriya, T. *Phys. Rev.* **1960**, *120*, 91−98.
(47) Schevciw, O.; White, W. B. *Mater. Res. Bull.* **1983**, *18*, 1059−1068.